Paper pa02-070
Submitted to the 28th International Conference on High Energy Physics
ICHEP'96, Warsaw, Poland, July 1996

A Measurement of the Proton Structure Function $F_2(x, Q^2)$ at Low x and Low Q^2 at HERA

H1 Collaboration

Abstract:

Preliminary results on a measurement of the proton structure function $F_2(x, Q^2)$ are reported for momentum transfers squared Q^2 between 0.35 GeV^2 and 3.5 GeV^2 and for Bjorken x values down to $6 \cdot 10^{-6}$ using data collected by the HERA experiment H1 in 1995. The data represent an increase in kinematical reach to lower x and Q^2 values of about a factor of 5, compared to previous H1 measurements. The F_2 is found to flatten off with x for the lowest Q^2 values. The data are compared with low Q^2 phenomenological models.

1 Introduction

The measurement of the inclusive deep inelastic lepton-proton scattering (DIS) cross section has been of great importance for the understanding of quark-gluon substructure of the proton [1]. Recently published measurements on the structure function F_2 at HERA based on analyses of the 1994 data cover the range in squared momentum transfer (Q^2), Bjorken-x and inelasticity ($y = Q^2/xs$) corresponding to $1.5 < Q^2 < 5000$ GeV^2, $3 \cdot 10^{-5} < x < 0.32$ and roughly $y > 0.01$ [2, 3]. These data have shown that F_2 persists to rise with decreasing x for the lowest Q^2 values reached, contrary to expectations of bare Regge phenomenology [4]. In terms of W, the invariant mass of the $\gamma^* p$ system (at low x, $W \simeq \sqrt{Q^2/x}$), F_2 is related to the total cross-section of the proton-virtual photon interaction ($\sigma_{tot}(\gamma^* p)$) via

$$\sigma_{tot}(\gamma^* p) \simeq \frac{4\ \pi^2 \alpha}{Q^2} F_2(W, Q^2). \tag{1}$$

The F_2 growth can be contrasted with the weak rise with W of the total real photoproduction ($Q^2 = 0$) cross-section in the same range of W : 20-225 GeV [5, 6]. The photoproduction data are well described by Regge inspired models. The persistent rise of F_2 at low x, when going down in Q^2 indicates that the photoproduction region has not been reached yet.

The data presented in this paper extends the Q^2 region in a continuous way down to lower Q^2 values, and allows to study if the deep inelastic approach more the photoproduction limit, and whether a transition region is reached. This extension could be achieved by using the detector upgrade in the backward (electron direction) region. A new calorimeter and tracking chamber with increased acceptance for small scattering angles have been installed in the winter shutdown 94/95. Together with a 70 cm shift of the main collision vertex in the proton direction, the data have an acceptance in Q^2 down to $Q^2 \sim 0.3$ GeV^2. In this paper we present data for the kinematic range $0.35 < Q^2 < 3.5$ GeV^2 and $x > 6 \cdot 10^{-6}$, and compare the result with Regge inspired and QCD models.

The structure function $F_2(x, Q^2)$ is derived from the inclusive lepton-proton scattering cross section. In 1995 the incident electron energy was $E_e = 27.5$ GeV and the proton energy was $E_p = 820$ GeV, leading to a total centre of mass energy of the collision $\sqrt{s} = 300$ GeV. The data were recorded with the H1 detector, which is described in [7]. A salient feature of the HERA collider experiments is the possibility of measuring not only the scattered electron but also the complete hadronic final state, apart from losses near the beam pipe. This means that the kinematical variables x, y and Q^2 can be determined with complementary methods which experimentally are sensitive to different systematic effects. These methods were exploited and detailed already in [8, 2] describing the analysis of the 1993 and 1994 data.

2 The H1 Detector

The H1 detector [7] is a nearly hermetic multi-purpose apparatus built to investigate the inelastic high-energy interactions of electrons and protons at HERA. The structure function measurement relies essentially on the tracking chamber system and on the backward calorimeter and the liquid argon calorimeters which will be described here briefly.

The tracking system includes the central tracking chambers, the forward tracker modules and a backward drift chamber. These chambers are placed around the beam pipe at z positions between -1.5 and 2.5 m. A superconducting solenoid surrounding both the tracking system and the liquid argon calorimeter provides a uniform magnetic field of 1.15 T.

The central jet chamber (CJC) consists of two concentric drift chambers covering a polar angle range from 15^o to 165^o. Tracks crossing the CJC are measured with a transverse momentum resolution of $\delta p_T/p_T < 0.01 \cdot p_T/\mathrm{GeV}$. The CJC is supplemented by two cylindrical drift chambers at radii of 18 and 47 cm, respectively, to improve the determination of the z coordinate of the tracks. A proportional chamber is attached to each of the z drift chambers for triggering.

A tracking chamber system made of three identical modules measures hadrons emitted in the forward direction (7^o to 20^o). The forward tracker is used to determine the vertex for the events which leave no track in the CJC. This allows an extension of the analysis to larger x values.

In the backward region a four module drift chamber (BDC) [9] was located with a polar angle acceptance of 151^o to 178^o, for collisions at the nominal vertex. For data with the vertex shifted by 70 cm in the proton direction the large angle acceptance increases to 178.6^0. The BDC provides track segments for charged particles entering the backward calorimeter. These are used to identify electrons and to measure θ_e, together with the event vertex reconstructed from tracks in the forward and central tracker. The resolution for reconstructed BDC hits is about 0.5 mm in the radial direction R, and 2.5 mm in the azimuthal angle ϕ.

In the backward region a lead/scintillating fiber calorimeter (SPACAL) [9] was installed, replacing the previous lead/scintillator electromagnetic calorimeter (BEMC). The new calorimeter has both an electromagnetic and hadronic section. The angular acceptance of the SPACAL is $153^0 < \theta < 177.8^0$ for collisions at the nominal vertex, increasing to 178.5^0 for collisions where the interaction vertex is shifted by 70 cm in the proton direction. The relative energy resolution measured from scattered electrons during the experiment operation is $7.8\%/\sqrt{E(\mathrm{GeV})}$ (preliminary) for the electromagnetic calorimeter. The absolute energy scale is determined to be 1-3%. The high readout granularity (1192 channels) results in an angular resolution of 1-2 mrad. Around the beampipe the electromagnetic section of the SPACAL has a veto layer (inner and outer radius 5.7 cm and 6.5 cm respectively), used to detect clusters for which the shower can have a large leakage out of the detector. The hadronic section has 136 channels. The hadronic energy scale uncertainty on the measurement in the SPACAL is presently about 10%. Both calorimeter parts have a time resolution of better than 1 ns which reduces considerably proton beam induced background.

Hadronic final state energies are further measured in the liquid argon (LAR) calorimeter [10] which covers an angular region between 3^o and 155^o. The calorimeter consists of an electromagnetic section with lead absorber plates and a hadronic section with stainless steel absorber plates. Both sections are highly segmented in the transverse and longitudinal directions with about 44000 cells in total. The electromagnetic part has a depth between 20 and 30 radiation lengths. The total depth of both calorimeters varies between 4.5 and 8 interaction lengths.

The luminosity was determined from the measured cross section of the Bethe Heitler (BH) reaction $ep \to ep\gamma$. The final state electron and photon can be detected in calorimeters (electron and photon "taggers") close to the beam pipe but at large distances from the main detector (at $z = -33$ m and $z = -103$ m).

3 Monte Carlo Programs

Monte Carlo DIS events corresponding to two times the luminosity of the data were generated using DJANGO [11]. The program is based on HERACLES [12] for the electroweak interaction and on LEPTO [13] to simulate the hadronic final state. HERACLES includes first order radiative corrections, the simulation of real bremsstrahlung photons and the longitudinal structure function. The acceptance corrections were performed using a parametrization the GRV[14] parton distributions as initial structure function for the Monte Carlo calculations. For very low Q^2 values (below 0.8 GeV^2) a phenomenological parametrization is used for the low x region. LEPTO uses the colour dipole model (CDM) as implemented in ARIADNE [15] which is in good agreement with data on the energy flow and other characteristics of the final state as measured by H1 [16] and ZEUS [17].

Photoproduction background was simulated based on the PHOJET [18] generator for γp interactions. A sample of photoproduction events was generated which contained all classes of events (elastic, soft hadronic collisions, hard scattering processes and heavy flavour production), corresponding to 1.5 times the luminosity of the data. PHOJET was used for events with $Q^2 < 0.1$ GeV^2, and DJANGO for events with $Q^2 > 0.1$ GeV^2 for acceptance and background calculations. The results were checked not to depend on the exact value of this Q^2 value.

Based on the GEANT program [19] the detector response was simulated in detail. After this step the Monte Carlo events were subject to the same reconstruction and analysis chain as the real data.

4 Kinematics and Event Selection

A data sample corresponding to an integrated luminosity of 120 nb^{-1} has been analysed and will be presented here. For this data sample the interaction vertex was shifted by 70 cm in the proton direction. The kinematic variables of the inclusive scattering process $ep \rightarrow eX$ can be reconstructed in different ways using measured quantities from the hadronic final state and from the scattered electron. The choice of the reconstruction method for Q^2 and y determines the size of systematic errors, acceptance and radiative corrections. The basic formulae for Q^2 and y used in the different methods used are given in [8]. The methods used in the analysis of the 1995 data are: i) the so called "electron method" (E), using only the information of the scattered electron, which has the best resolutions on x and Q^2 at large y; ii) the so called "Σ method", (Σ), calculated from the electron and hadronic final states measurements, which has small radiative corrections and extends from very low to large y values. Both calorimetric and track information are used to calculate the kinematics with the Σ method. The application of different methods was important to check that the systematic errors were correctly evaluated.

To reduce the systematic errors of the F_2 measurement, data taking periods with high quality data were selected based on the behaviour of the main detector components. The number of accepted events per luminosity was checked to be constant within statistical errors during the full data taking period.

The luminosity was determined from the measured cross section of the Bethe Heitler reaction $e^+p \to e^+p\gamma$, measuring the hard photon bremsstrahlung data only. The precision of the luminosity determination for these shifted vertex position data amounts to 1.1% [20].

The events were obtained by a calorimetric trigger in SPACAL (energy threshold> 4 GeV) of a signal in time with an ep collision. The trigger efficiency is basically 100% for electrons with an energy above 7 GeV, the lowest electron energy value used for this analysis.

Deep inelastic events are selected, for which:

- the most energetic cluster in SPACAL is an electron candidate (see below) and the timing of its signals is within a window of 11 ns around the expected value for a genuine ep collision;
- a reconstructed interaction vertex from the central or forward tracker which is within 30 cm of the average vertex position along the beam (z) direction;
- for the electron method analysis a total amount of $\Sigma(E_i - P_{i,z})$ larger than 35 GeV is required, with E_i and $P_{i,z}$ the energy and longitudinal momentum of a particle. The sum runs over all particles measured with the calorimeter.

An electromagnetic cluster in the SPACAL is considered as an electron candidate if following requirements are fulfilled:

- the energy of the cluster must be larger than 7 GeV;
- the radius of the electromagnetic cluster must be smaller than 3.5 cm;
- a matching track segment in the BDC to the cluster in the SPACAL must exist within 2 cm along R and 2.5 cm along ϕ from the cluster; The segment closest to the cluster is used for the calculation of θ_e
- the distance of the track, projected onto the SPACAL surface, to the beamline should be larger than 8.7 cm, corresponding roughly to an acceptance of $\theta_e < 178$.
- less than 1 GeV of energy should be deposited in the veto layer of the SPACAL, to avoid having too much leakage close to the beampipe
- the energy measured behind the shower in the hadronic part of the SPACAL, within a radius of 17.5 cm of the projected shower center, should be less than 0.5 GeV.

At low Q^2 the main sources of non-ep background are due to proton beam interactions with residual gas and beam line elements upstream of the H1 detector. An efficient reduction of the remaining background is provided by the minimum energy and the vertex requirements discussed above. The residual background was estimated to represent less than 2% of the total number of events at high y, as found by visual inspection.

The only significant background to DIS from ep interactions is due to photoproduction events at $Q^2 \simeq 0$ where the scattered electron escapes the detector along the beam pipe but in which an energy cluster from the hadronic final state fakes an electron. For About 10% of these events the scattered electron is detected in the electron tagger, and these events can be identified as photoproduction background. To estimate the full photoproduction background, photoproduction events corresponding to the luminosity of the data were generated with the Monte Carlo program PHOJET[18] and the H1 detector response was simulated in detail. The result is shown in Fig. 1, where the energy spectrum of the downstream electron tagger and the energy of the (fake) electron candidate in the SPACAL are shown for tagged photoproduction events for data and Monte Carlo predictions. The photoproduction background was subtracted statistically bin by bin. For each Q^2 value bin, only the smallest x point has a contamination larger than 5%. This contamination never exceeds 20% in any bin.

Fig. 2 shows the energy and angular distribution of electron candidates in the DIS selected sample, together with Monte Carlo predictions for the sum of DIS and photoproduction background. The structure function of the Monte Carlo calculation is reweighted as described in Section 5. A good agreement is observed between data and Monte Carlo calculations. Fig. 3 shows the distribution of $\Sigma(E_i - P_{z,i})$ for the full data sample and for the sample with $y > 0.55$. The Monte Carlo describes the data reasonably well. The level to which the hadronic variables are under control is demonstrated in Fig. 4, where the distributions of the ratio of the y values measured with the Σ and E method y_Σ/y_e and the transverse momentum of the hadronic system and the scattered electron $p_{t,h}/p_{t,e}$ are shown. Here the data are limited to $y_\Sigma > 0.05$ to ensure a good quality reconstruction of the kinematics with the electron method. In all, the detector response is demonstrated to be well under control.

5 Structure Function Measurement

The structure function $F_2(x, Q^2)$ was derived after radiative corrections from the one-photon exchange cross section

$$\frac{d^2\sigma}{dxdQ^2} = \frac{2\pi\alpha^2}{Q^4 x}(2 - 2y + \frac{y^2}{1+R})F_2(x, Q^2). \qquad (2)$$

Compared to the previous H1 analysis [2] the F_2 measurement has been extended to lower Q^2 (from 1.5 GeV^2 to 0.35 GeV^2), and to lower x (from $3 \cdot 10^{-5}$ to $6 \cdot 10^{-6}$). The determination of the structure function requires the measured event numbers to be converted to the bin averaged cross section based on the Monte Carlo acceptance calculation. The data were binned in a grid of $Q^2 - x$ bins for the region $Q^2 > 0.75$ GeV^2, in order to study the Q^2 evolution of F_2, and a grid of $Q^2 - y$ bins for the region below 0.75 GeV^2, which is more optimal to reach the smallest possible Q^2, x values. All detector efficiencies were determined from the data utilizing the redundancy of the apparatus. Apart from very small extra corrections all efficiencies are correctly reproduced by the Monte Carlo simulation. The bin averaged cross section was corrected for higher order QED radiative contributions, the longitudinal structure function (see below), and a bin centre correction was performed. This determined the one-photon exchange cross section which according to eq.(2) led to the values for $F_2(x, Q^2)$.

A first determination of the F_2 values uses an F_2 parametrization in the Monte Carlo simulation as given in Section 3. With those results a new QCD fit was made on proton data which includes furthermore results from E665[21], and BCDMS[22]. The starting value for the evolution Q_0^2 was taken to be 0.35 GeV^2. The fit is found to be too low for the low x data for $Q < 1$ GeV^2. Therefore this fit was only taken for the data with $Q > 1$ GeV^2, and for the high x part of the data at lower Q^2 values. For the low x part in this Q^2 region a modified version of the two parameter phenomenological fit was taken [23], where the parameters were determined in an iterative procedure [1].

The structure function ratio $R = F_2/2xF_1 - 1$ has not been measured yet at HERA for the very low Q^2 region. The following assumption was taken for R in this analysis. For $Q^2 \geq 0.85$ GeV^2 R was calculated from the QCD relation [14, 24] using the parton parametrization from the QCD fit above. For the region $Q^2 < 1$ GeV^2 a VMD inspired function is used which interpolates between the value $R(Q^2 = 1\text{GeV}^2)$ and $R = 0$ for $Q^2 = 0$:

$$R = R(1\text{GeV}^2) \cdot Q^2(Q_1^2 + m_\rho^2)/(Q_1^2(Q^2 + m_\rho^2)) \tag{3}$$

where m_ρ^2 is the mass of the ρ meson and $Q_1^2 = 1$ GeV^2. The Monte Carlo curves discussed in Section 4, in comparison with data, are reweighted with the F_2 and R functions as given above.

For the final values of the structure function F_2 presented below, R was taken as described above for $Q^2 \geq 0.85$ GeV^2 and put to zero for smaller Q^2 values. Only the lowest x point in each Q^2 bin is affected significantly by R. For $Q^2 \geq 0.85$ GeV^2, the effect of R leads to a correction of 10-15% at smallest x (and at most a few % elsewhere); for $Q^2 < 0.85$ GeV^2 assuming instead of $R = 0$, R as given by the prescription above, leads to an increase of F_2 for the lowest x points by approximatively 10%.

A list of the systematics errors for F_2 with preliminary, conservative values is given below.

- A potential miscalibration of the electron energy in the SPACAL, varying from 1.5% at large electron energies to 3% at 8 GeV.
- A 4% scale error for the hadronic energy in the LAr calorimeter, the effect of which is reduced due to the joint consideration of tracks and calorimeter cells for the Σ analysis. A 10% scale error was assigned to the energy of the hadronic final state measured in the SPACAL.
- A shift of up to 1 mrad for the electron polar angle.
- For the electron identification efficiency, for each cut the error was taken to be 50% of the fraction of events lost by the cut as given by the DIS Monte Carlo, or the difference between data and (DIS + γp) Monte Carlo of the total amount of events lost due to the cut. Apart from the electron identification all efficiencies were determined from the data and compared with the Monte Carlo simulation. The following contributions from the event selection were included: vertex efficiency: 3%; BDC efficiency: 3%; trigger and timing veto: 0.5%.
- An error of up to 2% in the radiative correction due to uncertainties from the hadronic corrections, the cross section extrapolation towards $Q^2 = 0$, second order corrections and the absence of the soft photon exponentiation in the HERACLES Monte Carlo.
- The uncertainty due to photoproduction background was assumed to be 30% of the correction applied, i.e. smaller than 6%. This affects only the highest y bins at lower Q^2.

[1] compared to [23] $\ln Q^2/\Lambda^2$ was replaced by $\ln{(Q^2 + Q_0^2)}/\Lambda^2$

- The total normalization uncertainty is 3% and results from the error on the luminosity and correction for satellite bunches, which lead to collisions about 70 cm displaced w.r.t. the main part of the bunch.

These systematic uncertainties affect differently the F_2 measurement made with different methods. In Fig. 5 the comparison of the measurement done with the E and with the Σ method is shown, with the full errors. The agreement between the two data sets is very good and well within the errors.

The two measurements are combined using the E method for the whole range available, adding Σ points at low y. The result is shown in Fig. 6. The measurements have a typical (preliminary) systematic error of 10-20%. Statistical errors in the Monte Carlo acceptance and efficiency calculations were computed and added quadratically to the statistical error of the data.

In Fig. 7 the data are shown as a function of Q^2 for different x-bins. Strong scaling violations are observed at small x.

In Fig. 8 the new data are compared with previous measurements of H1, measurements of E665, NMC [25] and ZEUS (preliminary)[26], and with predictions of models for F_2 at low-x. The results are in good agreement with the previous H1 publication [2]. The data also show a smooth continuation from the fixed target measurements and are compatible with the ZEUS measurements. It is seen that the rise at low x is still clearly present for $Q^2 \geq 0.85$ GeV^2, but becomes less steep for decreasing Q^2, to vanish almost completely at the lowest Q^2 values reached. This is also demonstrated in Fig. 9, where values of λ are shown from fits of the form $x^{-\lambda}$ to the F_2 data in each Q^2 bin. The data show that λ continues to decrease with decreasing Q^2, compared to the data of the 1994[2]

Parametrizations motivated by Regge theory relate the structure function to Reggeon exchange phenomena which successfully describe the slow rise of the total cross section with the centre of mass system energy in hadron-hadron and γp interactions. Using the "bare" instead of the "effective" pomeron intercept, the CKMT [27] parametrization rises faster with x compared to former DOLA [4] calculations. The Regge inspired models generally undershoot the data, except for the smallest Q^2 values where the calculations are in accord with the data. Some freedom exists in the CKMT model to improve the agreements with data in the region $Q^2 < 2$ GeV^2.

In Fig. 8 also the predictions from the GRV model are shown. This model assumes that all parton distributions at very low $Q_0^2 = 0.34$ GeV^2 have a valence like shape, i.e. vanish for $x \rightarrow 0$. Assuming that the leading twist QCD evolution equations can be used to evolve the parton distributions from this low Q_0^2 scale to larger Q^2 values, they predicted that the structure function F_2 should rise towards low x even for low values of $Q^2 \sim 1$ GeV^2 [14]. Fig. 8 shows that the GRV distributions describe the data well for $Q^2 \geq 1$ GeV^2, but systematically undershoot the data for $Q^2 < 1$ GeV^2. Hence it turns out that the kinematic region studied here is a meeting ground for Regge inspired models, which describe the data at the low Q^2 end, and models based on pQCD, which account well for the high Q^2 end. Such a model is the one of Badelek and Kwiecinski (BK [28]) which combines the concepts of Vector Meson Dominance with dynamical partons models such as the GRV[14] parton distributions. It has per force a smooth transition from pQCD to the real photon limit, which essentially coincides with the region studied here. The BK model is found to describe the data very well[2] Hence the data presented in this paper can be interpreted as constituting a transition region between DIS and photoproduction.

6 Summary

A measurement has been presented of the proton structure function $F_2(x, Q^2)$ in deep inelastic electron-proton scattering at low Q^2 with data taken in the running period of 1995 at HERA. First structure function measurements are shown made with the upgraded backward calorimeter and drift chamber.

The F_2 values presented are obtained using different methods to reconstruct the inclusive scattering kinematics. As the main method the electron method is used which is based on the scattered electron energy and angle. Lower y values are covered with the Σ method which combines electron and hadronic information to reduce radiative corrections and calibration errors. The data cover the region of Q^2 between 0.35 GeV^2 and 3.5 GeV^2 and for Bjorken x values down to $6 \cdot 10^{-6}$. The data show a smooth transition from the fixed target high x data to the HERA low x data, and are in accord with the ZEUS data at very low Q^2 values

The distinct rise of the structure function with decreasing x in the low x region, very prominent for $Q^2 > 2$ GeV^2 is reduced strongly with decreasing Q^2. The rise observed at the smallest values of Q^2 reached is close to the one expected from Regge parametrizations. Hence the data cover a region where a smooth transition from DIS to photoproduction is observed.

Acknowledgements

We are very grateful to the HERA machine group whose outstanding efforts made this experiment possible. We acknowledge the support of the DESY technical staff. We appreciate the big effort of the engineers and technicians who constructed and maintained the detector. We thank the funding agencies for financial support of this experiment. We wish to thank the DESY directorate for the support and hospitality extended to the non-DESY members of the collaboration.

References

[1] for recent reviews see: F. Eisele, Proceedings of the 1995 International Europhysics Conference on High Energy Physics, Brussels, DESY-95-229;
A. Caldwell, Proceedings of the 1995 International Symposium on Lepton and Photon Interactions at High Energies, Beijing, DESY-95-231.

[2] H1 Collab., S. Aid et al., Nucl. Phys. B470 (1996) 3.

[3] ZEUS Collab., M. Derrick et al., DESY preprint 96-76

[2] note that the lowest x data points in the 3 low Q^2 bins increase by about 10% in case a VDM prescription for R is taken

[4] A. Donnachie and P. V. Landshoff,Z. Phys. **C61** (1994) 139.

[5] H1 Collab., T. Aid et al., Z. Phys. **C69** (1995) 27.

[6] ZEUS Collab., M. Derrick et al, Z. Phys. **C63** (1994) 408

[7] H1 Collab., I. Abt et al., DESY report H1-96-01 (1996) submitted to Nuclear Instruments and Methods.

[8] H1 Collab., T. Ahmed et al., Nucl. Phys. **B439** (1995) 471.

[9] H1 Collab. Technical Proposal for the Upgrade of the Backward Region of the H1 Detector, DESY internal report PRC-93/02.

[10] H1 Calorimeter Group, B. Andrieu et al., Nucl. Instr. and Meth. **A336** (1993) 460.

[11] G. A. Schuler and H. Spiesberger, Proceedings of the Workshop Physics at HERA, vol. 3, eds. W. Buchmüller, G. Ingelman, DESY (1992) 1419.

[12] A. Kwiatkowski, H. Spiesberger and H.-J. Möhring, Computer Phys. Comm. **69** (1992) 155.

[13] G. Ingelman, Proceedings of the Workshop Physics at HERA, vol. 3, eds. W. Buchmüller, G. Ingelman, DESY (1992) 1366.

[14] M. Glück, E. Reya and A. Vogt, Z. Phys **C67** (1995) 433;
We show the parametrizations as presented in:
A. Vogt, Proceedings of the Workshop on Deep-Inelastic Scattering and QCD, Paris (1995) 261,
using the NLO charm contribution as calculated in

[15] L. Lönnblad, Computer Phys. Comm. **71** (1992) 15.

[16] H1 Collab., I. Abt et al., Z. Phys. **C63** (1994) 377.

[17] ZEUS Collab., M. Derrick et al., Z. Phys. **C59** (1993), 231.

[18] R. Engel, Proceedings of the XXIXth Rencontre de Moriond, ed. J. Tran Thanh Van, (edition frontieres, 1994) 321.

[19] R. Brun et al., GEANT3 User's Guide, CERN–DD/EE 84–1, Geneva (1987).

[20] H1 Collaboration Luminosity Measurement in the H1 Experiment at HERA (submitted to ICHEP96: pa17-026).

[21] E665 Collaboration, M.R. Adams et al., FNAL-Pub-95/396-E (1995).

[22] BCDMS Collaboration, A.C. Benvenuti et al., Phys. Lett. **B223** (1989) 485;
CERN preprint CERN-EP/89-06.

[23] A. De Roeck, M. Klein and T. Naumann, DESY preprint 96-063 (1996).

[24] G. Altarelli and G. Martinelli, Phys. Lett. **B76** (1978) 89.

[25] NMC Collaboration, M. Arneodo et al., Phys. Lett. **B364** (1995) 107.

[26] W. Zhu, to appear in the proceedings of the Workshop DIS96, Rome, edt. G. D'agostini (1996).

[27] A. Capella et al., Phys. Lett. **B337** (1994) 358.

[28] B. Badelek and J. Kwiecinski, Phys. Lett. **B295** (1992) 263.

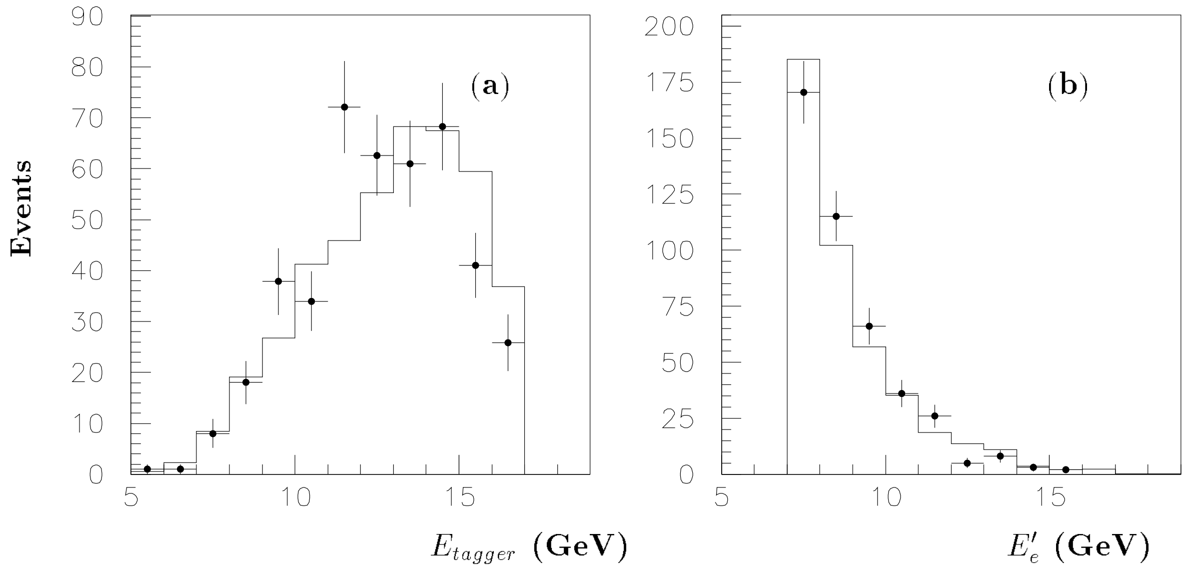

Figure 1: *Experimental (points) and Monte Carlo (solid lines) distributions of* a) *the energy in the electron tagger b) the energy of the electron candidate in the SPACAL, for tagged photoproduction events.*

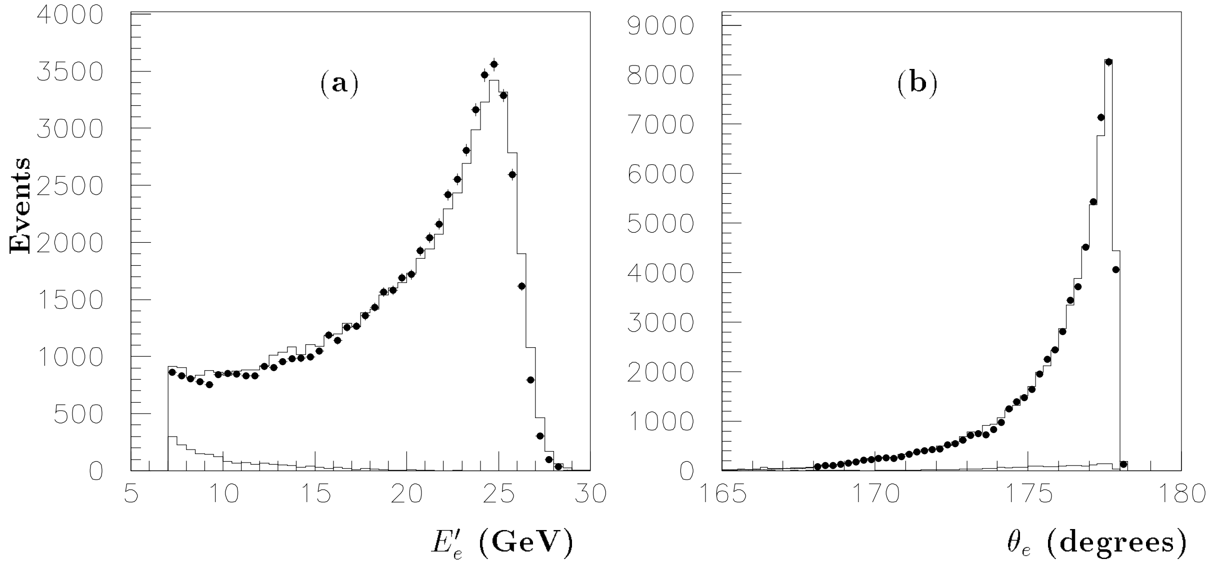

Figure 2: *Experimental (points) and Monte Carlo (solid lines) distributions of* a) *the energy of the scattered electron and* b) *the polar angle of the scattered electron for DIS events. The Monte Carlo curve is the sum of DIS and photoproduction events (shown seperately by the lower curve).*

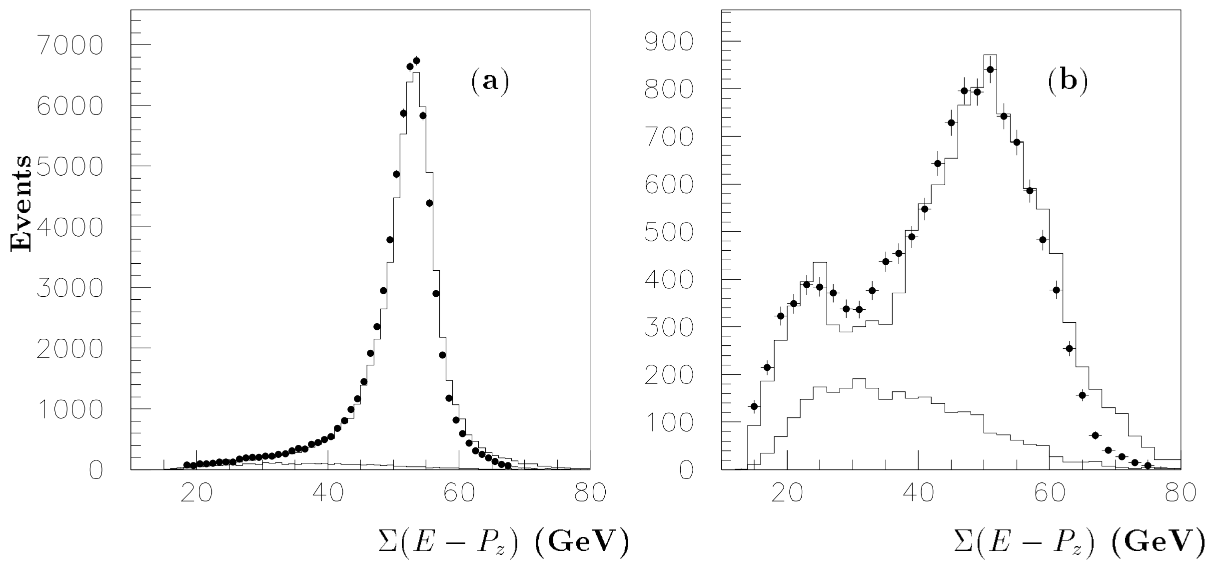

Figure 3: *Experimental (points) and Monte Carlo (solid lines) distributions of* $\Sigma(E_i - P_{z,i})$ *measured in the calorimeter for* a) *all DIS event candidates,* b) *DIS event candidates with* $y > 0.55$. *The Monte Carlo curve is the sum of DIS and photoproduction events (shown separately by the lower curve)*

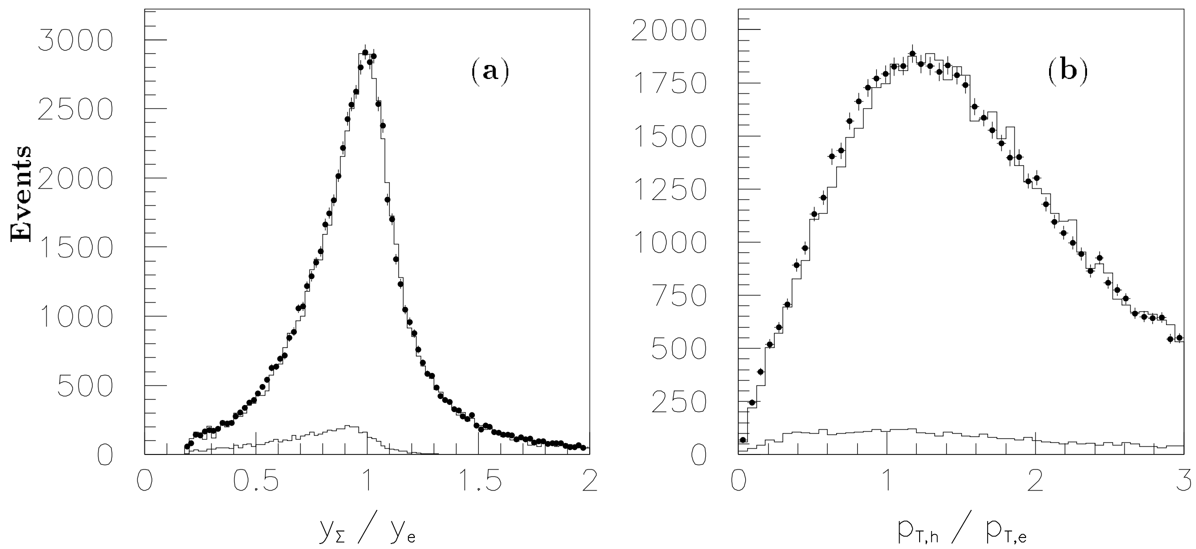

Figure 4: *Experimental (points) and Monte Carlo (solid lines) distributions for* $y_\Sigma > 0.05$ *of the ratio of* a) *the* y *values measured with the Sigma, and Electron method* y_Σ/y_e*, and* b) *the transverse momentum of the hadronic system and the electron* $p_{t,h}/p_{t,e}$*. The Monte Carlo curve is the sum of DIS and photoproduction events (shown separately by the lower curve)*

H1 PRELIMINARY

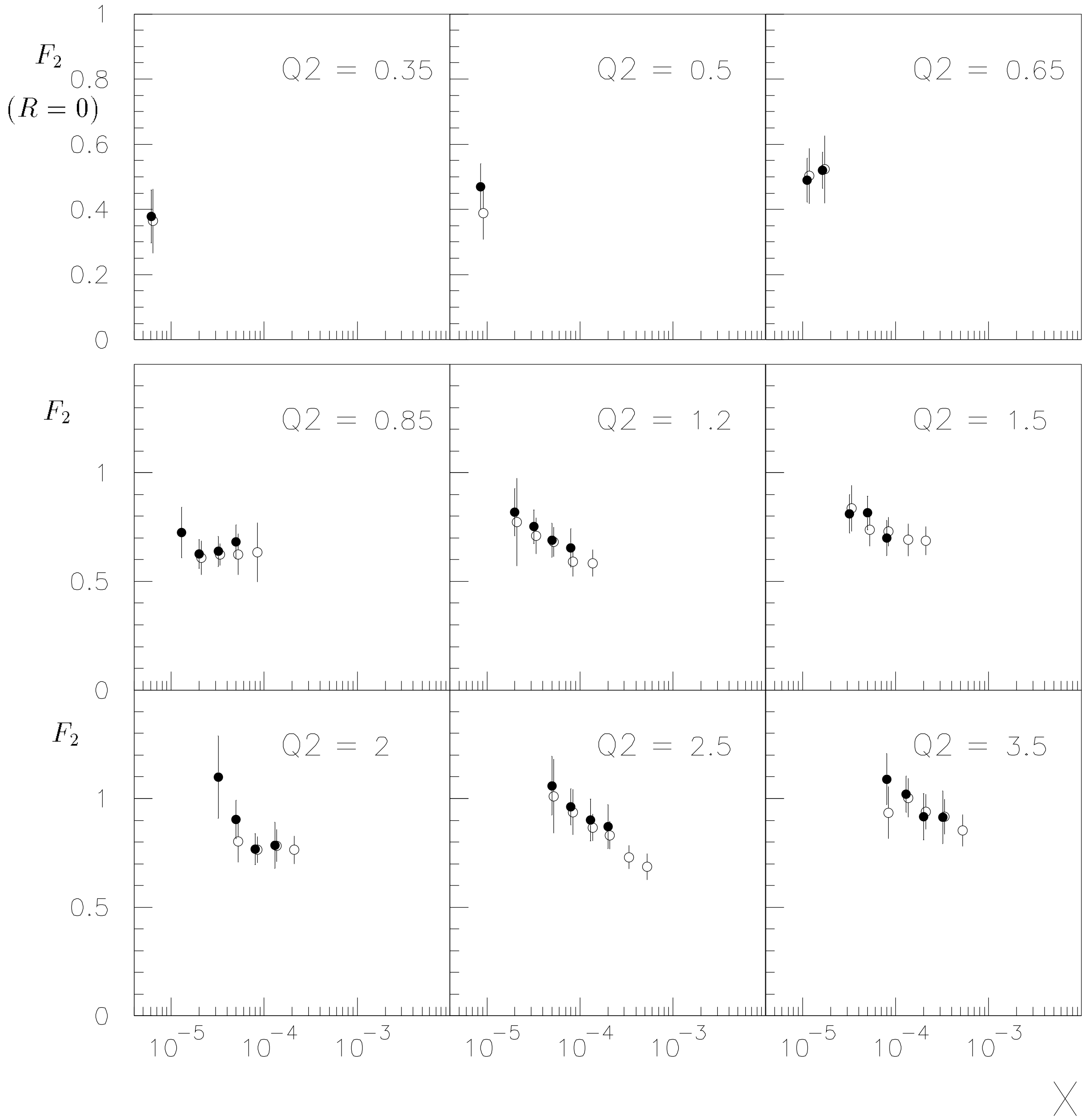

Figure 5: *Comparison of the proton structure function $F_2(x,Q^2)$ (preliminary) as function of x in different bins of Q^2 measured with the E method (full points) and with the Σ method (open points). The full error represents the statistical and systematic errors added in quadrature.*

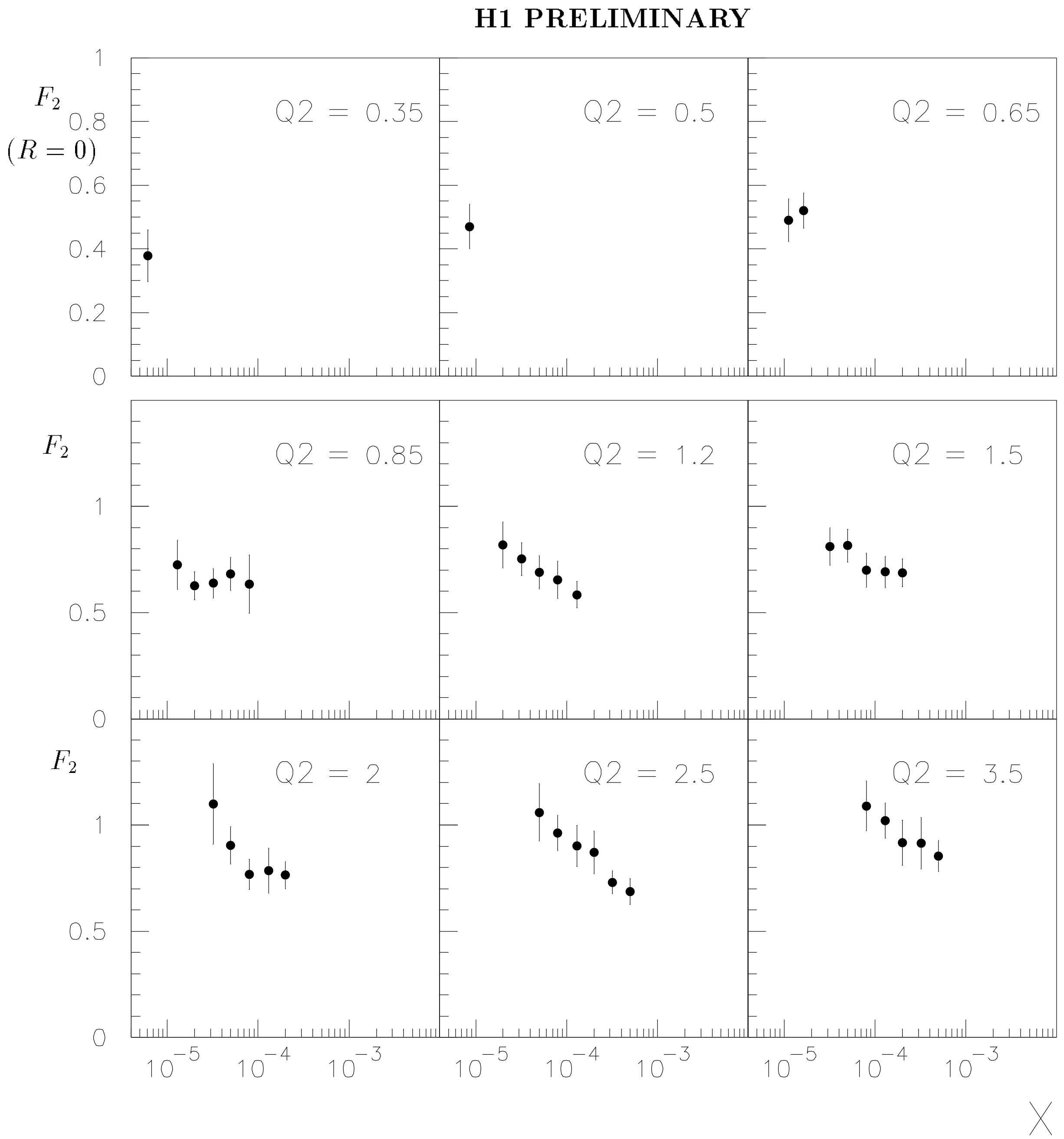

Figure 6: *Preliminary measurement of the proton structure function $F_2(x, Q^2)$ as function of x in different bins of Q^2. The error represents the statistical and systematic errors added in quadrature.*

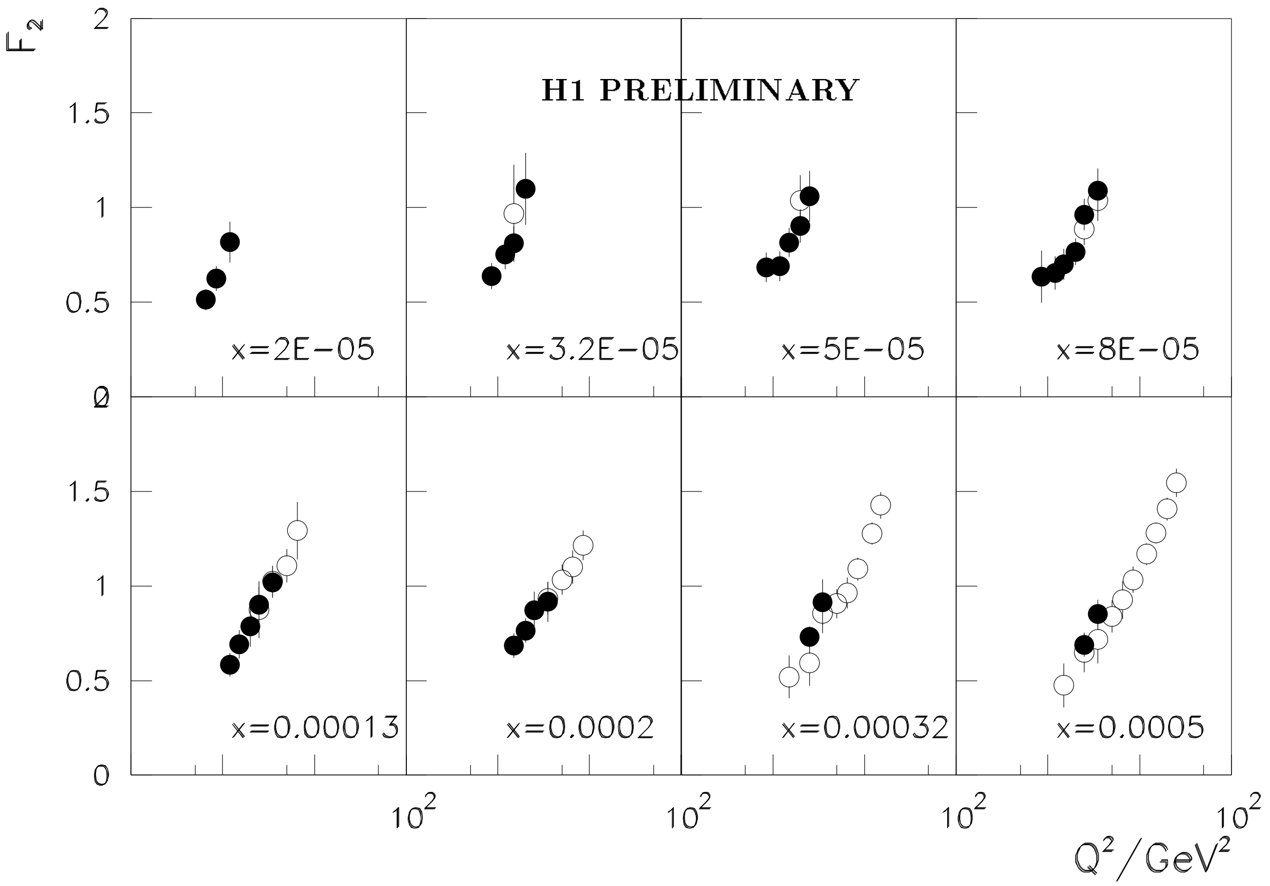

Figure 7: *Preliminary measurement of the proton structure function* $F_2(x, Q^2)$ *as function of* Q^2 *in different bins of* x*. The error represents the statistical and systematic errors added in quadrature. Full symbols are data from this analysis; open symbols are data from [2].*

H1 PRELIMINARY

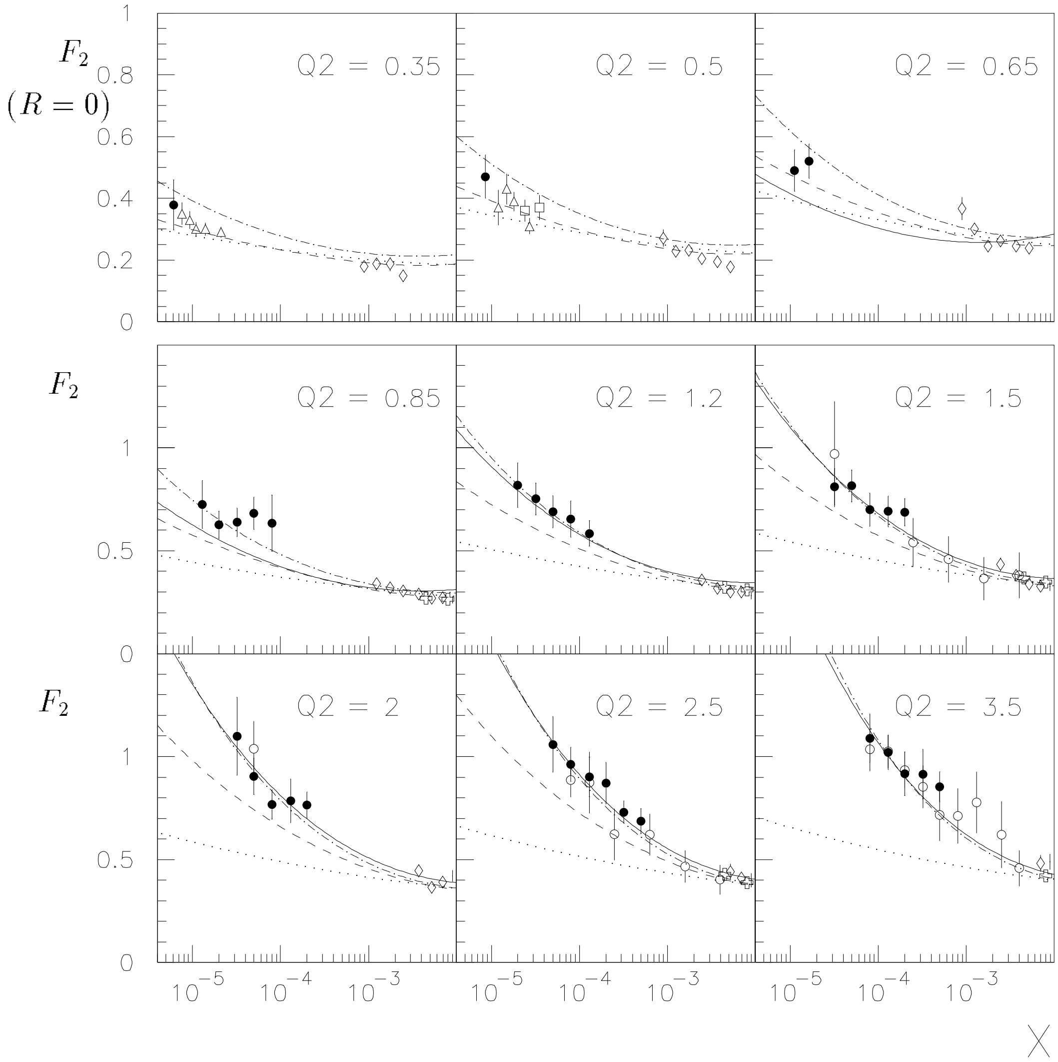

Figure 8: *Preliminary measurement of the proton structure function $F_2(x, Q^2)$ in the low Q^2 region by H1 (full points), together with results from the E665 experiment (open diamonds), NMC (open crosses) and ZEUS (open squares and triangles). The ZEUS data are bined differently: data of ZEUS shown in the $Q^2 = 0.5$ GeV^2 bin correspond to a value of $Q^2 = 0.44$ GeV^2 (triangles) and $Q^2 = 0.57$ GeV^2 (squares) respectively. Different predictions for F_2 are compared to the data the model of Donnachie and Landshoff (dotted line), the CKMT model (dashed line), the model of Badelek and Kwiecinski (dashed doted line) and the model of Gluck, Reya and Vogt (full line).*

H1 PRELIMINARY

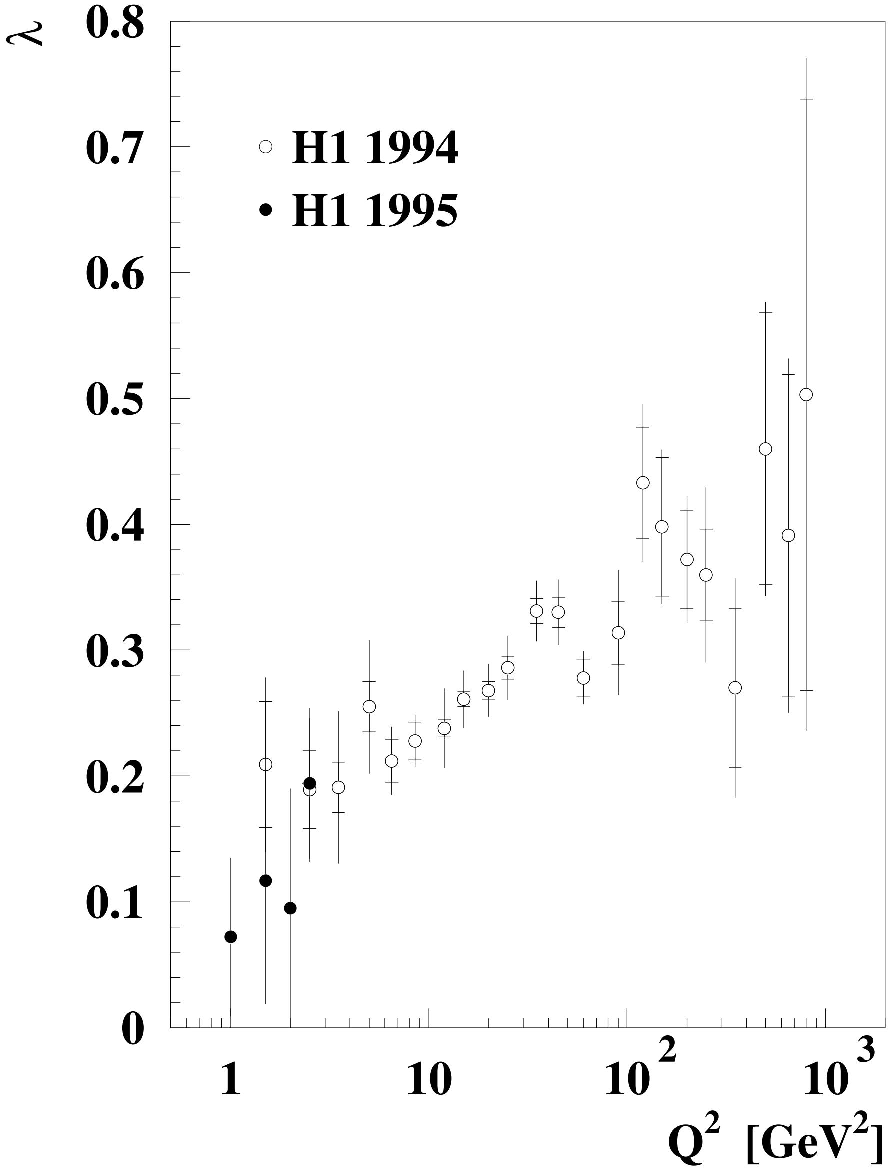

Figure 9: *Variation of the exponent λ from fits of the form $F_2 \sim x^{-\lambda}$ at fixed Q^2 values and $x < 0.1$. Full symbols are the data from this analysis; open symbols are the data from [2].*